Sustainable Energy & Fuels

ROYAL SOCIETY OF CHEMISTRY

PAPER

View Article Online
View Journal | View Issue

Cite this: *Sustainable Energy Fuels*, 2025, **9**, 3041

Enhancing the performance of Ni-rich Li[$Ni_{0.88}Co_{0.09}Mn_{0.03}$]$O_2$ cathode material using surface coating

Hossein Rostami, *[ab] Parisa Mehdipour,[ab] Tao Hu, [a] Palanivel Molaiyan,[a] Pekka Tynjälä[ab] and Ulla Lassi [ab]

Nickel-rich layered oxide cathodes are becoming increasingly popular for use in lithium-ion batteries (LIBs). However, their widespread application faces challenges due to rapid capacity degradation and poor performance at low temperatures, prompting the development of protective coatings. Wet methods and atomic layer deposition are complex and time-consuming, potentially causing lithium deficiencies. Therefore, this study proposes a facile and cost-effective powder dry coating strategy using a high-energy mixer for the surface modification of $LiNi_{0.88}Co_{0.09}Mn_{0.03}O_2$ (NCM-88) with graphene oxide (GO). The nanostructured GO layer applied to the NCM-88 surface effectively protects the cathode particles. Various characterization techniques, such as scanning electron microscopy (SEM), transmission electron microscopy (TEM), X-ray diffraction (XRD), and X-ray photoelectron spectroscopy (XPS), confirm the successful synthesis of GO and uniform coating on NCM-88 particles without altering pristine morphology. Based on the electrochemical test results, the optimized GO coatings exhibit a significant improvement in rate performance and capacity retention. Electrochemical characterization shows that coated NCM-88 with 0.2 wt% GO exhibits the best performance, with an initial discharge capacity of 221.1 mA h g^{-1} at 0.1C and a capacity retention of approximately 97% after 50 cycles at 2C. In comparison with other studies, the NCM-88 coated with 0.2 wt% GO exhibits superior electrochemical performance, achieving a remarkable discharge capacity of 171.3 mA h g^{-1} at 1C after 1000 cycles with 90.3% capacity retention, which significantly exceeds the stability and retention rates of pristine and various modified NCM compositions reported in the literature. These results demonstrate the effectiveness of GO surface modification for enhancing the electrochemical performance of NCM-88 cathodes in LIBs.

Received 13th January 2025
Accepted 10th April 2025

DOI: 10.1039/d5se00052a

rsc.li/sustainable-energy

1. Introduction

The global energy crisis and concerns about climate change are fueling the rapid growth of the electric vehicle market, leading to increasing pressure on current energy storage technologies.[1] Extensive research has been conducted on advanced energy storage technologies such as solar cells, batteries, supercapacitors.[2–4] Among a large number of energy storage technologies, lithium-ion batteries (LIBs) have been considered as suitable power sources for electric vehicles and hybrid electric vehicles (HEVs) owing to their high energy density, and long cycle life.[5,6] Among all the components of LIBs, the cathode is crucial, serving as the main source of lithium ions and a determinant of capacity and cost. Developing cathode materials with safety, affordability, high performance, and high capacity will facilitate the widespread use of LIBs.[7,8]

Compared to other cathode materials such as $LiCoO_2$, $LiFePO_4$, and $LiMn_2O_4$, layered $LiNi_xCo_yMn_{1-x-y}O_2$ (NCM) offers a higher theoretical capacity, operating voltage, and cycling stability, making it a promising candidate material for commercial LIBs.[9] Nowadays, a series of NCM cathode compositions have been investigated, including $LiNi_{1/3}Co_{1/3}Mn_{1/3}O_2$ (NCM111), $LiNi_{0.5}Co_{0.3}Mn_{0.2}O_2$ (NCM532), $LiNi_{0.6}Co_{0.2}Mn_{0.2}O_2$ (NCM622), $LiNi_{0.8}Co_{0.1}Mn_{0.1}O_2$ (NCM811), and $LiNi_{0.88}Co_{0.09}Mn_{0.03}O_2$ (NCM-88). However, the higher Ni content in NCM causes structural instability and capacity fading. This is due to irreversible phase transitions, side reactions at the electrode/electrolyte interfaces, and the loss of electrical contact from anisotropic volume changes.[10] In general, cation mixing (Ni^{2+} migration to Li^+ sites) leads to the phase transition of Ni-rich NCM during charging from a layered structure ($R\bar{3}m$) to spinel ($Fd\bar{3}m$) and rock-salt ($Fm\bar{3}m$) structures. This structural instability hinders Li^+ transport, and the electrolyte is broken down by oxygen released during the transformation, creating a resistive layer at the electrode/electrolyte interface. Furthermore,

[a]*Research Unit of Sustainable Chemistry, University of Oulu, P.O. Box 3000, FI-90014 University of Oulu, Finland. E-mail: H.rostami64@gmail.com; Hossein.rostamimalkhalifeh@oulu.fi*

[b]*University of Jyvaskyla, Kokkola University Consortium Chydenius, Talonpojankatu 2B, FI-67100 Kokkola, Finland*

continuous lithiation/delithiation results in particle cracks, which also reduces particle contact and forms parasitic reaction sites along microcracks.[11–13]

Thus, many efforts have focused on developing effective modification strategies to address these obstacles and enhance the electrochemical efficiency of Ni-rich NCMs.[14] Element doping, surface coating, and the design of concentration gradient particles are common strategies used to improve the performance of NCMs by either coating their surfaces or doping them with additional substances.[15–17] Surface modification can isolate NCM surfaces from electrolytes, thereby minimizing undesirable side reactions such as the dissolution of transition metal cations, oxygen release, and phase conversion.[18] Therefore, different coating materials, such as Al_2O_3,[19] zeolite ZSM-5,[20] MgO,[21] Al_2O_3/$LiAlO_2$,[22] Li_2TiO_3,[23] TiO_2,[24,25] V_2O_5,[26] ZrO_2,[27] polymers (*i.e.*, polyimide),[28] and [3-(trimethoxysilyl) propyl methacrylate],[29] have been employed to enhance the thermal stability and rate capacity. However, most metal oxides can lead to electrode polarization and decreased reversible capacity due to their inactivity in lithium insertion/extraction. Additionally, some modification techniques often require costly equipment or raw materials, hindering their practical commercial applications.[30] Due to their high electrical conductivity, large surface area, and structural mechanical stability, carbon-based materials are among the most promising cathode modification materials for LIBs.[31,32]

Nanocarbon materials like carbon fibers, carbon nanotubes (CNTs), carbon black, and graphene oxide (GO) have been extensively utilized.[33–39] Among them, CNTs and GO have attracted much attention because of their large surface area, strong electrical conductivity, and unique 1D tubular and 2D planar architectures.[40] There are two practical methods for surface modification with carbon materials: one utilizes carbon precursors, and the other uses carbon materials. However, carbon surface modification of Ni-rich NCM has constraints on the process, with methods using carbon precursors requiring high-temperature heating under an inert atmosphere to achieve the desired electrical conductivity.[41] Coating methods, such as wet coating or atomic layer deposition, are time-consuming and complex, potentially causing surface lithium deficiency and phase restoration. Therefore, this study demonstrates a dry, straightforward, and efficient method for surface modification of NCM-88 with GO. The nanostructured GO layer applied to the surface effectively protects the cathode particles. Electrochemical tests of the optimized coatings indicated a significant improvement in rate performance and capacity retention with an ideal amount of GO material.

2. Experimental

2.1 Synthesis of graphene oxide (GO)

To synthesize GO, an improved $NaNO_3$-free Hummer's method was used by partially replacing $KMnO_4$ with K_2FeO_4.[42] Briefly, 100 mL of concentrated sulfuric acid was mixed with 10 g of flake graphite, 6 g of $KMnO_4$, 4 g of K_2FeO_4, and 0.01 g of boric acid and stirred for two h at a temperature below 5 °C. After the addition of 5 g $KMnO_4$, the mixture was transferred to a water bath at 35 °C and stirred for an additional 3 h. Next, 250 mL of deionized water was gradually added, and the temperature was adjusted to 95 °C. The diluted mixture turned brown after 15 min, indicating complete exfoliation and hydrolysis of intercalated graphite oxide. Finally, to reduce the residual oxidants and intermediates to soluble sulfate, 12 mL of 30% H_2O_2 was added, and the mixture was centrifuged for 20 min to remove residual graphite. The product was washed repeatedly with 1.0 M HCl and deionized water to yield the final GO.

2.2 Surface modification of $LiNi_{0.88}Co_{0.09}Mn_{0.03}O_2$ using GO

NCM-88 precursors were synthesized based on our previous literature using the hydroxide coprecipitation method from $MeSO_4$ solutions, with NaOH and NH_3 as chelating agents at 50 °C under inert conditions. After filtration, the precursor dried overnight in a vacuum oven at 60 °C and mixed with 5% excess LiOH, the material was calcined at 780 °C in an oxygen atmosphere, then milled and sieved for final processing.[20] $Li(Ni_{0.88}Co_{0.09}Mn_{0.03})O_2$ (NCM-88) was used as the cathode active material (CAM), and nanostructured GO powder was used as coating material during the dry coating process. First, NCM-88 was combined with GO and ground to ensure appropriate blending. Subsequently, the dry-coating alteration of the blending occurred within a high-energy mixer equipped with rapidly rotating rotors and blades. The powders were mixed with different amounts of GO (0.1 wt%, 0.2 wt%, 0.5 wt% and 1.0 wt%) *via* mixer at the acceleration of high mix and then calcined to achieve a well-distributed coating on the surface of the CAM. Fig. 1 depicts a diagram illustrating the procedure for dry coating of NCM-88 with GO. The slurry was composed of 4 wt% polyvinylidene fluoride (Kureha #1100), 4 wt% carbon (Timcal C45), and 92 wt% active material (NCM-88), with 1-methyl-2-pyrrolidinone (NMP, Alfa Aesar, anhydrous 99.5%) as the solvent. The mixture was mixed using a Thinky ARE-250 mixer. The slurry was applied to an aluminum foil using 100 μm applicators and dried on a hot plate at 50 °C for one hour, followed by drying in a vacuum oven at 120 °C overnight. The cathode foil was then calendered three times before being assembled into coin cells of the 2016-type format. GO-coated NCM-88 cathodes with coating amounts of 0.1 wt%, 0.2 wt%, 0.5 wt% and 1.0 wt% were denoted as NCM-88/0.1%, NCM-88/0.2%, NCM-88/0.5% and NCM-88/1%, respectively.

2.3 Characterization of the precursors and cathode powders

X-ray diffraction (XRD) measurements were conducted using Rigaku SmartLab 9 kW X-ray diffractometers with a Co source at 40 kV and 135 mA. Diffractograms were collected in the 2θ range of 5–120° at 0.01° intervals, with a scan speed of 4.06° per minute. The peaks were identified using the International Center for Diffraction Data (PDF-4+ 2023) database. Crystallite sizes, anisotropy, and distribution were computed using Rigaku PDXL2 analysis software, employing the Whole Powder Pattern Fitting (WPPF) method, decomposition, and the least square Pawley method. Peak shape was modeled using the Fundamental Parameter (FP) method with continuous scan and the Cheary–Coelho axial model. The crystallite shape was refined as

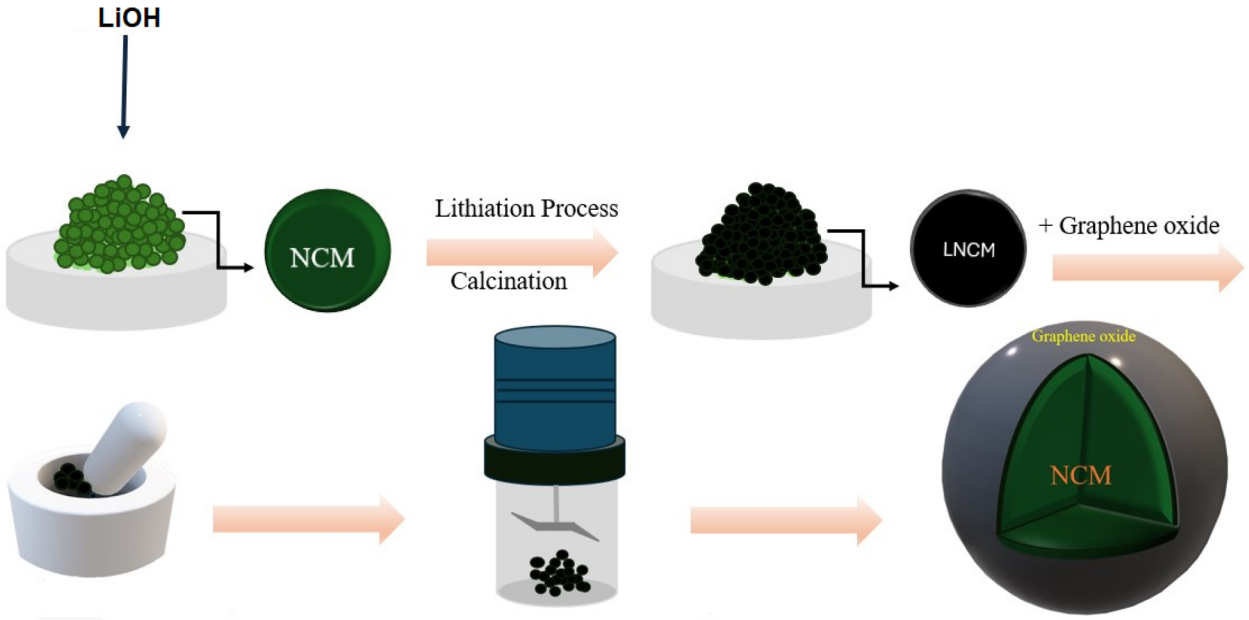

Fig. 1 Schematic representation of the process of dry coating of NCM-88 with GO.

ellipsoidal, and the lognormal distribution was used as a free parameter for iterative refinement. Site occupancy was analyzed using the Rietveld model provided by PDXL2.

Microstructures from field-emission scanning electron microscopy (FESEM) images were obtained using a Zeiss Sigma FESEM instrument operating at 5 kV. The morphology and microstructure of GO-coated NCM-88 particles were studied using a JEOL JEM-2200FS energy-filtered transmission electron microscope (EFTEM) equipped with a scanning transmission electron microscopy (STEM). A thin layer sample for TEM analysis was prepared using a focused ion beam (FIB) technique and then cut to obtain a thin layer of around 100 nm. TEM images were performed in STEM mode with an accelerating voltage of 120 kV and an emission current of 8–15 μA. XRD, TEM, and FESEM analyses were performed at the Centre for Material Analysis at the University of Oulu.

X-ray photoelectron spectroscopy (XPS) was used to analyze the chemical environment at the surface (with a thickness of less than 10 nm) using a Thermo Fisher Scientific ESCALAB 250Xi XPS system (Thermo Fisher Scientific, Waltham, MA, USA). The powder samples were placed in a gold sample container. A survey scan was conducted with a pass energy of 150 eV, while a high-resolution scan used a pass energy of 20 eV. The system utilized monochromatic Al Kα radiation (1486.7 eV) with an X-ray spot size of 900 μm, operating at 20 mA and 15 kV. Measurements were performed for Li, Ni, Al, O, and C across all samples. The data were analyzed using Thermo Fisher Scientific's Avantage v.5 software. The binding energies were calibrated, and the spectra were determined by using the C 1s peak at 284.8 eV for charge compensation.

2.4 Electrochemical characterization

Electrode foils and battery cells were prepared in a dry room environment. For the coin cells, NCM-88 cathode electrode (14 mm) used as an active material metallic lithium (12 mm) served as the counter electrode, and the electrolyte was 1 M $LiPF_6$ in a 1 : 1 : 1 ratio of ethylene carbonate (EC), dimethyl carbonate (DMC), and ethyl methyl carbonate (EMC). The cells underwent 62 charge–discharge cycles at 25 °C at a specific C-rate. During charging, a constant current was applied until reaching 4.3 V, followed by a constant voltage phase until the current dropped to 0.015C for the first two cycles. For the subsequent cycles, the current threshold was increased to 0.02C. The first two discharge cycles were performed at a constant current of 0.1C until reaching 2.6 V, followed by a constant voltage phase until the current dropped to 0.015C. Afterwards, discharging to 3.0 V was carried out at a constant current. For the full cells, the cell included a graphite anode (Hitachi) and an electrolyte composed of 1.15 M $LiPF_6$ in a mixture of EC : DMC : EMC in a 2 : 4 : 4 ratio, along with 1 wt% vinylene carbonate. The N/P ratio was 1.19, with a cathode loading of 11 mg cm^{-2}, an anode loading of 7 mg cm^{-2}, and a capacity of 0.068 A h.

3. Results and discussion

3.1 Characterization of precursors and cathode samples

Fig. 2a displays the XRD patterns of the GO nanoparticles. The XRD spectra recorded in the range of 2θ from 6° to 70° show a (001) diffraction peak at $2\theta = 12.16°$ (d-spacing of 7.27 Å) and $2\theta = 26.36°$, indicating the distance between graphene layers.[43] In addition, the (100) diffraction peak at $2\theta = 42.52°$ according to a d-spacing of 2.13 Å, confirming the successful GO synthesis. Fig. 2b shows SEM images of graphene oxide. The SEM results revealed that the graphite peelings exhibited a layered configuration. The graphene oxide, in its altered state, displayed randomly arranged, sharply wrinkled sheets.

Fig. 3a depicts the XRD patterns of the uncoated and GO-coated NCM-88, showing highly distinct and well-defined

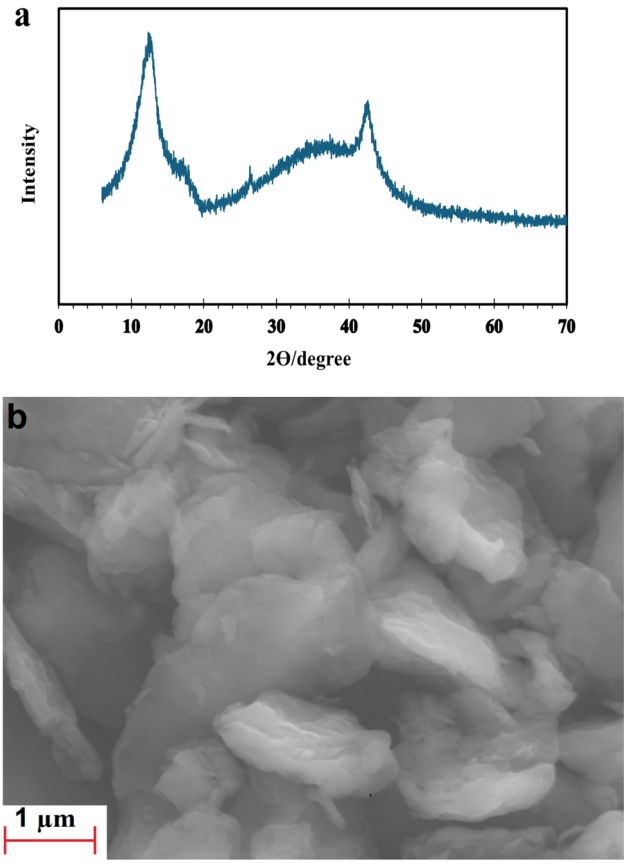

Fig. 2 (a) XRD pattern and (b) SEM image of graphene oxide.

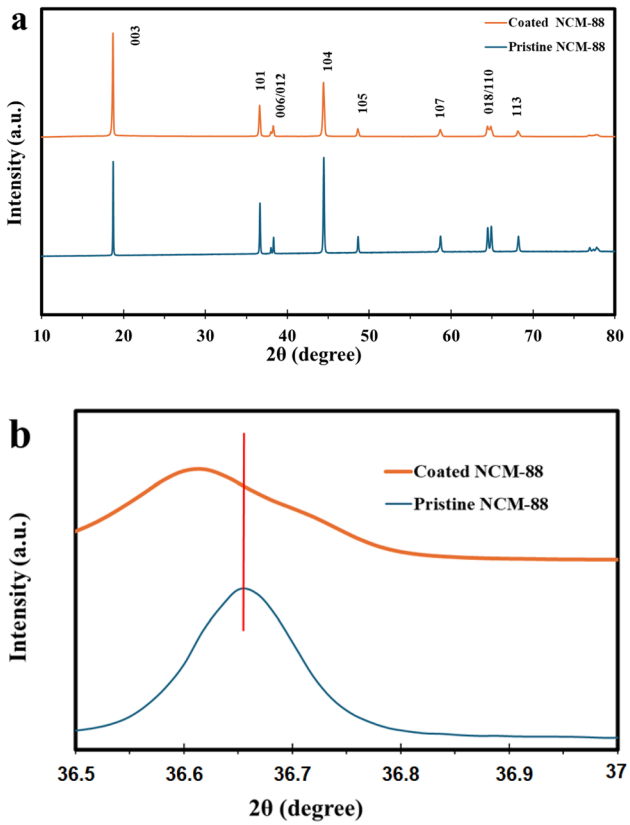

Fig. 3 (a) XRD patterns of pristine NCM-88 and GO-coated NCM-88/0.2%.

diffraction peaks. All the patterns exhibited a hexagonal α-$NaFeO_2$ structure, falling under the space group $R\bar{3}m$.[44] A minor peak shift was observed in the case of GO-coated NCM-88, for instance at a 2θ value of approximately 36.65°, indicating the partial impact of the GO coating, as illustrated in Fig. 3b. The observed peak splitting at 2θ angles of 38.5° and 65.4° can be attributed to the (006)/(012) and (018)/(110) planes of pristine NCM-88, respectively, suggesting the presence of a layered configuration. Furthermore, the absence of impurity peaks after GO coating suggested a high level of crystallinity and implies that the material could successfully retain its layered structure. In addition, the $(I_{003})/(I_{104})$ ratio in the diffraction pattern is a key element because it reflects the level of cation disorder between Li^+ and Ni^{2+} ions. This ratio directly influences the electrochemical characteristics, such as the initial charge and discharge specific capacity and cycling performance, with a higher ratio leading to improved performance.[45] In this study, the GO-coated sample showed $(I_{003})/(I_{104})$ values of 1.228, compared with 1.005 for the uncoated NCM-88. This indicates reduced Ni/Li disordering, which may explain the better electrochemical performance of GO-coated NCM-88 compared to that of pristine NCM-88. The values of $(I_{003})/(I_{104})$, a, c, and c/a for the samples are shown in Table 1. Notably, the GO-coated NCM exhibits the largest $I_{(003)}/I_{(104)}$ ratio and the highest c/a value, indicating that the GO coating is particularly effective in reducing cation mixing, optimizing the crystal's hexagonal structure, and facilitating ion diffusion. This suggests that the GO coating significantly enhances the structural stability and electrochemical performance of the material.

SEM was conducted to analyze the powder mixtures and assess whether the particles remained intact after coating. Fig. 4 demonstrates the morphology and microstructure of the coated NCM-88 sample. SEM images of the coated NCM-88 at different magnifications (Fig. 4a and b) show that the NCM particles remained intact after the coating process. The images also indicate that the GO coating did not alter the morphology of pristine NCM-88. The SEM images of the top surface of the electrode after the calendering steps (Fig. 4c and d) reveal a densely packed particle surface with an even distribution of particles across a large area of the electrode. This suggests that the dry GO coating process did not affect particle distribution. Based on the SEM images, there were no significant differences between the surface morphologies of the coated and uncoated particles.

The surface and structural characteristics of the GO-coated LNCM-88 were evaluated using TEM, and the results are shown in Fig. 4e and f. TEM images indicated that the particles were uniformly distributed, with no evidence of aggregation. According to the TEM images, a uniform amorphous coating layer is clearly visible, and the crystalline structure of NCM-88 remains intact. It is believed that this amorphous surface layer is graphene oxide, as shown in Fig. 4.

Table 1 Rietveld refinement results of NCM-88, and NCM-88/0.2% GO and, Ni, Co, and Mn concentrations

Sample	a (Å)	c (Å)	c/a	Volume	$I_{(003)}/I_{(104)}$	Ni (mol%)	Co (mol%)	Mn (mol%)	Ni/Li
Pristine NCM-88	2.8709	14.1913	4.9431	101.295	1.005	88.01	9.00	2.99	7.37
NCM-88/0.2% GO	2.8731	14.2394	4.9561	101.539	1.228	87.96	9.03	3.01	7.16

The surface valence states of NCM-88 before and after modification were analyzed by XPS, and the results are presented in Fig. 5. The XPS survey spectra of both coated and uncoated samples confirmed the presence of Li, Ni, Co, Mn, C, and O elements. High-resolution Ni 2p XPS spectra for all samples are shown in Fig. 5c and d. The peaks at about 856 eV

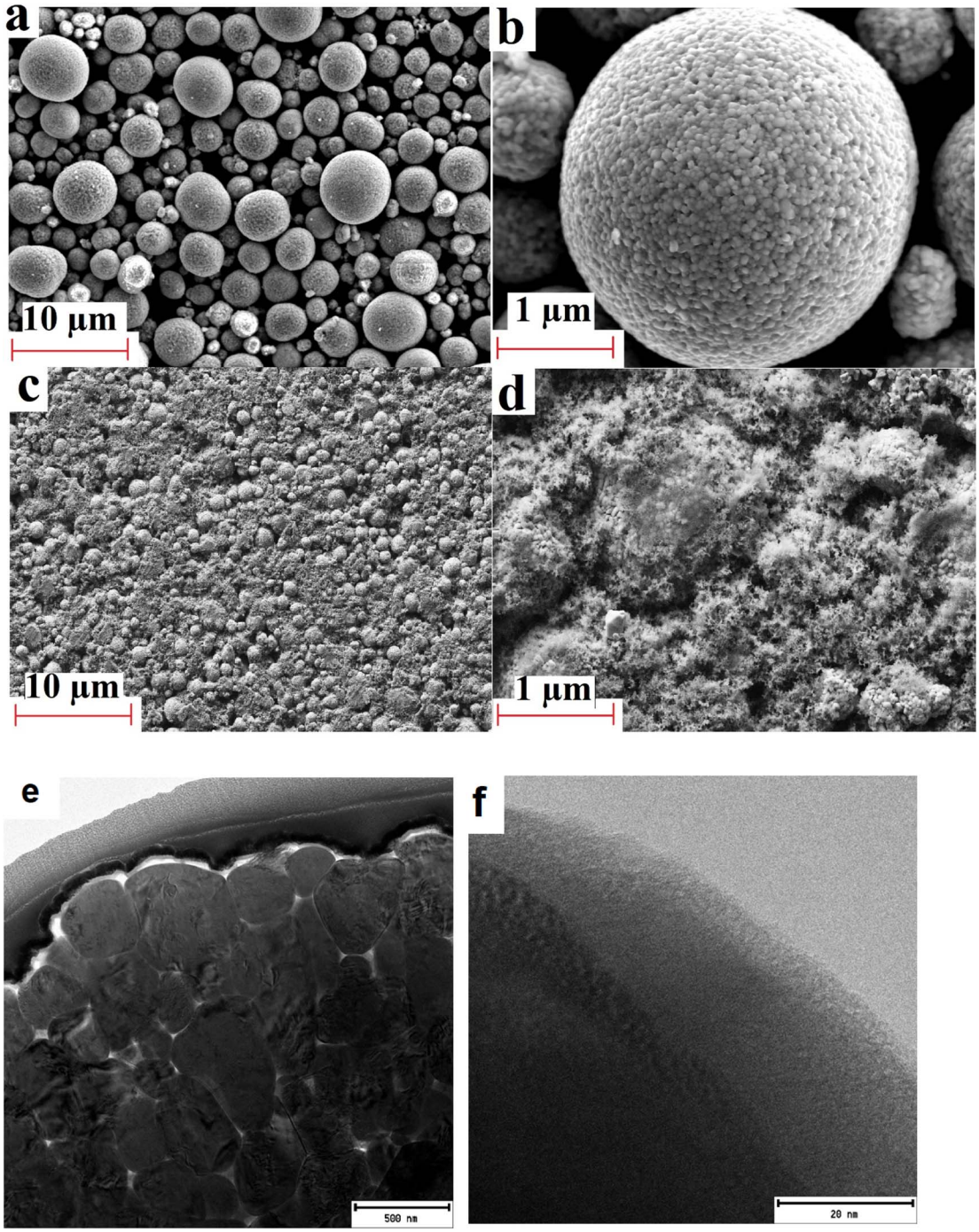

Fig. 4 SEM images of (a and b) NCM-88/0.2% sample after dry coating. (c and d) Coated NCM-88/0.2% slurry after drying and calendering. (e and f) TEM images of GO-coated NCM-88/0.2% sample at different magnifications.

correspond to Ni^{2+} ($2p_{3/2}$) and Ni^{3+} ($2p_{3/2}$), which is consistent with previous research.[46] It is confirmed that the spontaneous transformation from Ni^{3+} to Ni^{2+} on the surface of such Ni-rich layered materials can reduce the electrochemical performance of the cathode material.[47] A shift to a higher binding energy of 855.41 eV for the Ni $2p_{3/2}$ peak in the GO-coated NCM-88 sample (Fig. 5d), compared to 855.03 eV in the pristine NCM-88 (Fig. 5c), indicates a higher Ni^{3+}/Ni^{2+} ratio in the GO-coated NCM-88 and improved structural stability. Additionally, the binding energies in the Co 2p and Mn 2p XPS spectra of GO-coated NCM-88 were not different from those of pristine NCM-88. In the high-resolution O 1s spectra shown in Fig. 5e, two peaks are observed at approximately 529 eV and 531 eV. These peaks are attributed to lattice oxygen and surface impurities such as Li_2CO_3 and LiOH.[47] The intensity of the surface impurity peak in the GO-coated NCM-88 sample was significantly lower than that of the uncoated sample, demonstrating that GO can effectively protect the NCM-88 material. In the high-resolution Li 1s XPS spectra of pristine NCM-88 (Fig. 5f), the peaks at 54.2 eV and 55.2 eV can be related to $LiMO_2$ and Li_2CO_3 on the surface of the particles, respectively. In the XPS spectra of GO-coated NCM-88, the peak of $LiMO_2$ was not observed, indicating the presence of a coating on the surface of NCM-88.

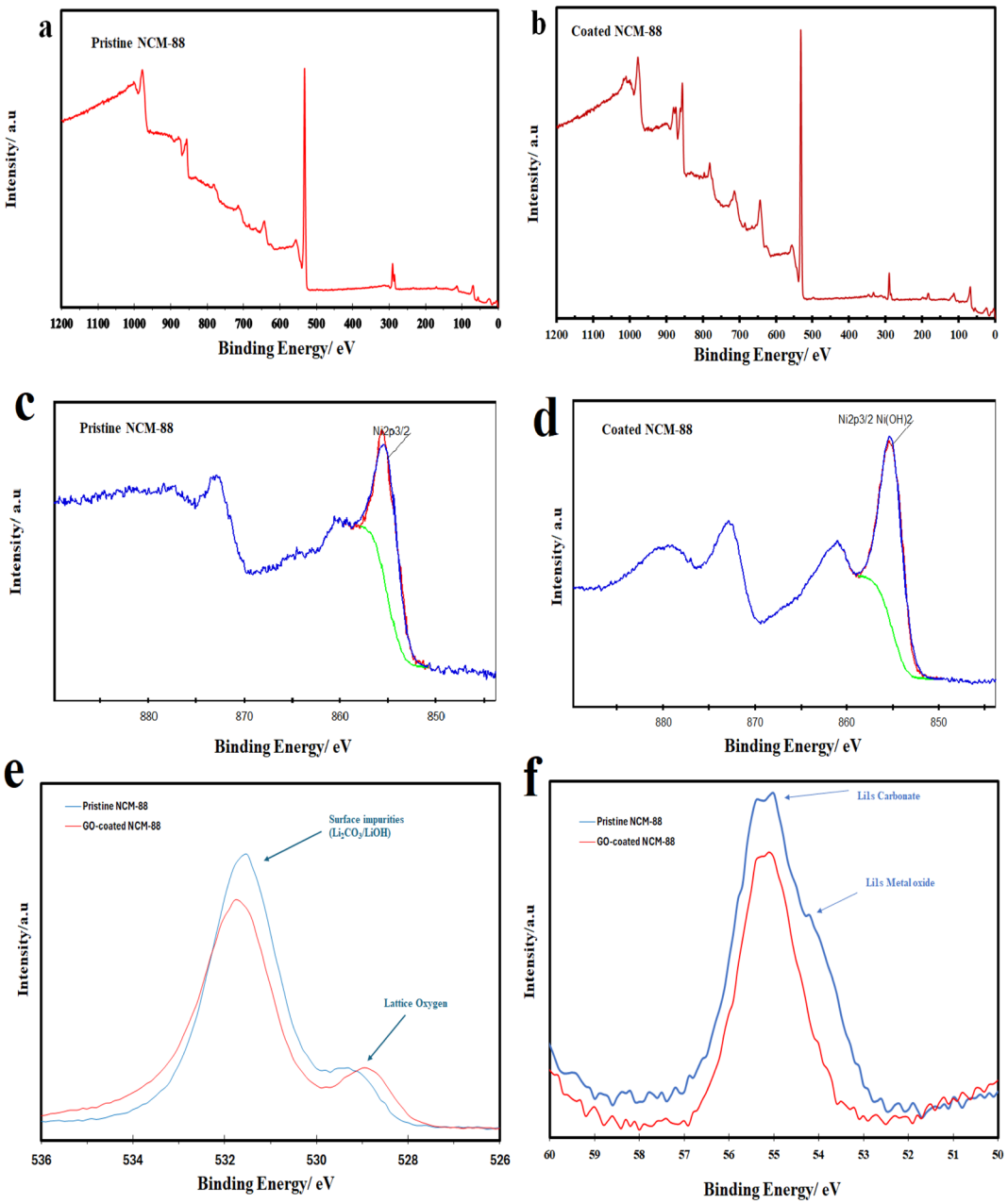

Fig. 5 XPS spectra of (a) the pristine and (b) GO-coated NCM-88/0.2% samples. High resolution of (c) Ni 2p of pristine and (d) GO-coated NCM-88. High resolution of (e) O 1s and (f) Li 1s of the pristine NCM-88 and GO-coated NCM-88 samples.

3.2 Electrochemical characterization of cathode materials

Galvanostatic charge/discharge measurements were conducted using coin cells to assess the electrochemical performance of the samples. The capacities for the first and 62nd cycles were measured for both coated and uncoated samples, with the results in Fig. 6. The first charge–discharge cycle of various cathode samples within the voltage range of 2.6 to 4.3 V (*vs.* Li/Li^+) at a charge/discharge rate of 0.1C (Fig. 6a). The uncoated NCM-88 cathode exhibited the lowest first-cycle charge and discharge capacity compared to the other samples. Specifically, the uncoated LNCM-88 showed a charge capacity of approximately 230.9 mA h g^{-1} and a discharge capacity of 210.5 mA h g^{-1} at 3.0 V. The GO-coated NCM-88 samples with 0.1, 0.2, 0.5, and 1 wt% coatings demonstrated similar electrochemical behavior to the bare NCM-88. The initial discharge capacities for the coated electrodes (0.1, 0.2, 0.5, and 1.0 wt%) at 3.0 V were 216.1, 218.2, 216.3, and 219 mA h g^{-1}, respectively. Among the different cathode materials, the NCM-88 coated with 1 wt% GO showed the highest charge capacity (240.6 mA h g^{-1}) and discharge capacity (219 mA h g^{-1}). The NCM-88 with a 0.2 wt% GO coating exhibited the most significant improvement in efficiency compared to the other NCM-88 cathodes. Table 2 shows that the coulombic efficiency (CE) remains relatively stable for all samples, ranging from 91.1% to 91.7%. The coated samples exhibit an improvement in CE compared to the uncoated NCM-88, with the highest value of 91.7% observed for the 0.2% coated sample. Fig. 6b shows the 62nd charge–discharge cycle at a rate of 0.1C. The results indicated that the NCM-88 with 1% GO coating exhibited a better discharge capacity of 217.5 mA h g^{-1} compared to the pristine NCM-88, which had a discharge capacity of 209.2 mA h g^{-1}. However, the retention rate after 62 cycles was approximately 99.31% for the NCM-88/1% sample, slightly lower than the 99.38% retention rate of the pristine NCM-88. The 62nd discharge capacities for the coated electrodes (0.1, 0.2, 0.5 and 1.0 wt%) were 213.6, 217.1, 211.3 and 211.5 mA h g^{-1}, respectively. Moreover, NCM-88/0.2% demonstrated better capacity retention of 99.5% after 62 cycles, compared to the pure NCM-88 under the same cycling conditions. Therefore, a GO coating thickness of 0.2 wt% is considered optimal for enhancing electrochemical performance. The Fig. 6c and d display dQ/dV plots for pristine NCM-88 and GO-coated NCM-88/0.2% at the 2nd cycle (c) and 62nd cycle (d). In the 2nd cycle, both samples exhibited sharp peaks, indicating well-defined redox reactions, with the GO coating having minimal impact. However, by the 62nd cycle, the pristine sample showed significant peak broadening and intensity reduction, suggesting greater degradation, whereas the GO-coated sample maintains clearer features, indicating improved stability. Voltage analysis further revealed that while both samples initially have similar peak positions, the pristine NCM-88 undergoes noticeable shifts after 62 cycles, reflecting increased polarization and resistance buildup. In contrast, the GO-coated sample retains more stable peak voltages, indicating reduced polarization and enhanced lithium-ion diffusion. These results suggest that GO coating enhances the structural and electrochemical stability of NCM-88 over extended cycling.

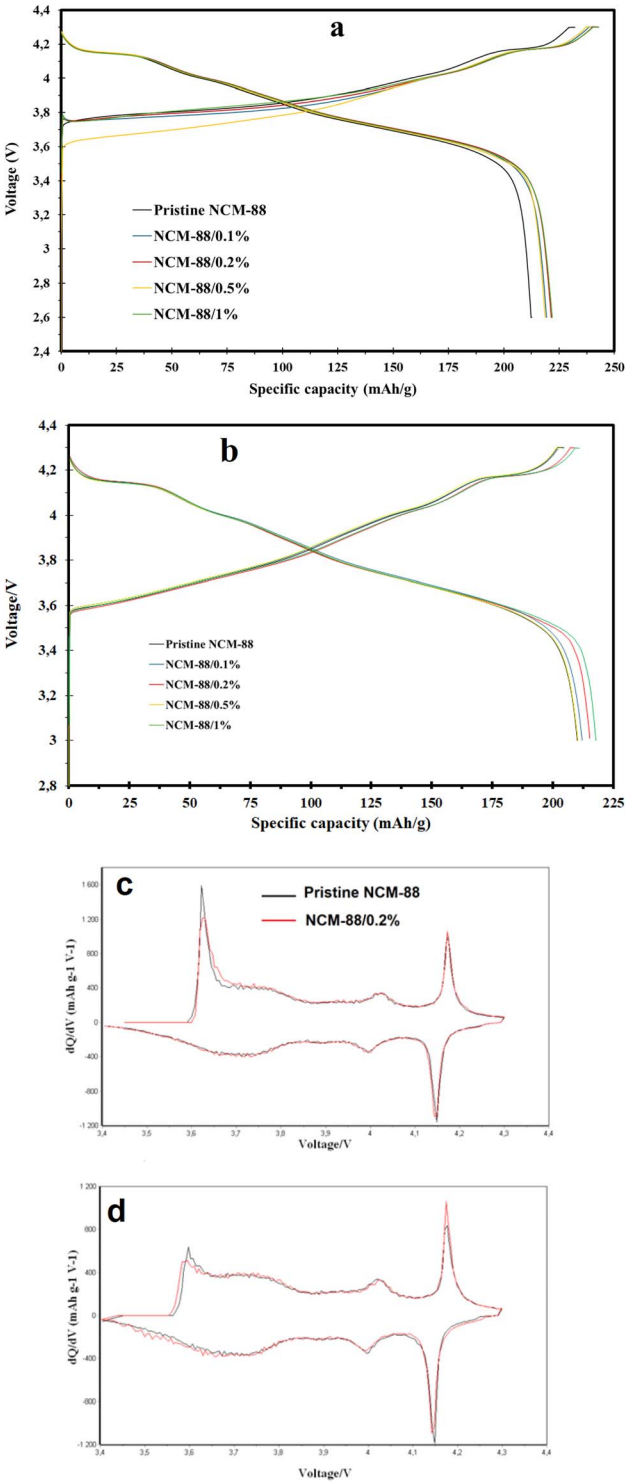

Fig. 6 Galvanostatic charge/discharge measurements at a charge/discharge rate of 0.1C: (a) initial charging/discharging and (b) charge and discharge curves after 62 charge and discharge cycles, (c and d) dQ/dV plots for pristine NCM-88 and coated NCM-88/0.2% at the 2nd cycle (c) and 62nd cycle (d).

Fig. 7a presents the results of the rate tests performed on uncoated and coated NCM-88 cells with varying percentages of GO coating. Each cell underwent a charging process at a rate of

Table 2 Electrochemical results of initial charge and discharge capacities and CE

Sample	0.1C charge, 1st (mA h g^{-1})	0.1C discharge, 1st at 3.0 V (mA h g^{-1})	Coulombic efficiency (%)
Uncoated NCM-88	230.9	210.5	91.1
NCM-88/0.1%	236.9	216.1	91.2
NCM-88/0.2%	238.0	218.2	91.7
NCM-88/0.5%	236.1	216.3	91.6
NCM-88/1%	240.6	219.0	91.2

0.1C before each discharge test, followed by discharge at different C-rates ranging from 0.1 to 2C. The discharge capacity *versus* discharge rate showed similar trends for all cathode materials, but the coated materials exhibited higher discharge capacities at all rates. This suggests that the coating improves performance. Although NCM-88/1% exhibited the highest specific capacity at a rate of 0.1C, the performance of samples with higher GO-percent coatings (NCM-88/0.5%, NCM-88/1%) significantly declined with increasing rates. Notably, at a high rate of 2C, NCM-88/0.2% outperformed the other samples. The NCM-88/0.2% sample demonstrated a discharge capacity of 188.6 mA h g^{-1} at 2.0C (compared to 221.1 mA h g^{-1} at 0.1C), achieving capacity retention of up to 85.3%, which is higher than the 84.2% retention observed for NCM-88/1%. Cycling performance was used to investigate the effectiveness of the coating by operating the cells at 2C and 25 °C, and results are given in Fig. 7b. The discharge cycling characteristics of cells assembled with uncoated NCM-88 and various coated NCM-88 cathode materials (Fig. 7b). The initial discharge capacities for pristine NCM-88, NCM-88/0.1%, NCM-88/0.2%, NCM-88/0.5%, and NCM-88/1% were 184.3, 187.4, 188.6, 186.5, and 186.0 mA h g^{-1}, respectively. After 50 cycles, the capacity retentions were 96.5% for bare NCM-88, 96.7% for 0.1 wt%, 97.0% for 0.2 wt%, 96.5% for 0.5 wt%, and 95.6% for 1 wt% GO-coated NCM-88. The electrochemical performance of bare NCM-88 is affected by several factors, including HF acid attacks caused by the anionic oxidation of PF_6^- and surface degradation with oxygen species, leading to electrode degradation and significant capacity fading. Among the samples, NCM-88/0.2% showed better electrochemical performance. This can be attributed to the superior ionic conductivity of the GO coating, which enhances Li^+ diffusion kinetics. Additionally, the coating helps mitigate cation mixing and increases lattice space within the optimized modified material. In contrast, the 0.5 wt% and 1 wt% GO-coated samples performed worse than the pristine NCM-88 and the NCM-88/0.2% samples. The lowered performance of NCM-88/0.1% compared to NCM-88/0.2% might be due to suboptimal coating, resulting in only minor improvements compared to the bare NCM-88. On the other hand, the thicker coating in the 0.5 wt% and 1 wt% samples likely hinders ion and electron movement to and within the active NCM-88 material, thereby limiting electrochemical performance. The 0.2 wt% GO coating is optimal, providing effective ion and electron transport and improving overall electrochemical performance.

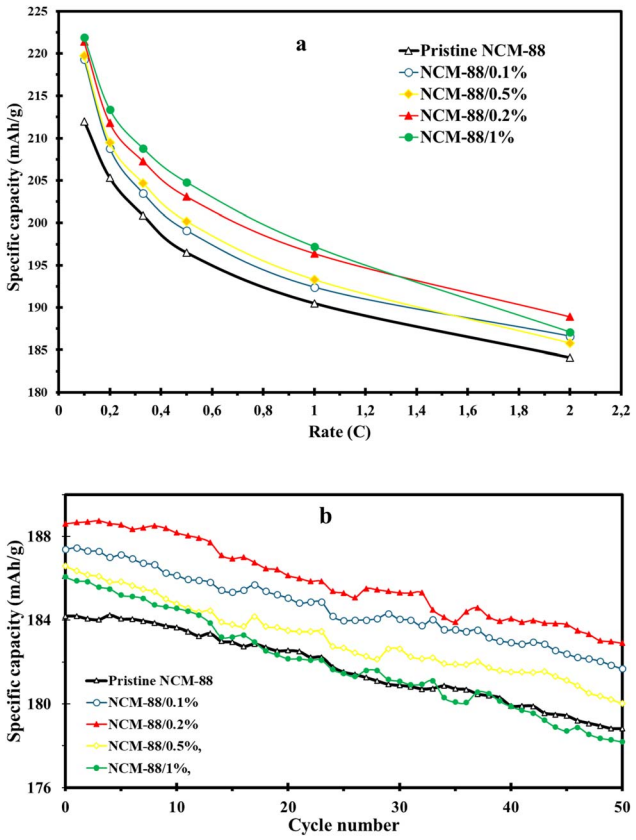

Fig. 7 Galvanostatic discharge measurements at (a) different C-rates ranging from 0.1 to 2C and (b) discharge cycling of uncoated NCM-88 and various coated NCM-88 cathode materials at 2C and 25 °C.

Lithium ions transferring within the constrained crystalline framework of cathode oxides often face diffusion challenges, leading to relatively limited kinetics compared to more flexible electrode systems, making rate capability a critical indicator for the practical application of Ni-rich cathode materials.[48] Fig. 10a illustrates pristine NCM-88 and coated NCM-88/0.2% rate capability behaviors. The rate capability performances of the electrodes were evaluated at different current rates of 0.015, 0.1, 0.2, 0.5, 1, and 2C. Among the various coated samples, the one with 0.2 wt% GO showed better rate performance, delivering capacities of 227.8, 220.2, 209.8, 204.7, 195.2, and 188.1 mA h g^{-1} at 0.015, 0.1, 0.2, 0.5, 1, and 2C, respectively. In contrast, the uncoated NCM-88 exhibited discharge capacities of 219.2, 213.1, 204, 197.3, 188.4, and 182.8 mA h g^{-1} at the same current rates. The rate performance studies indicate that

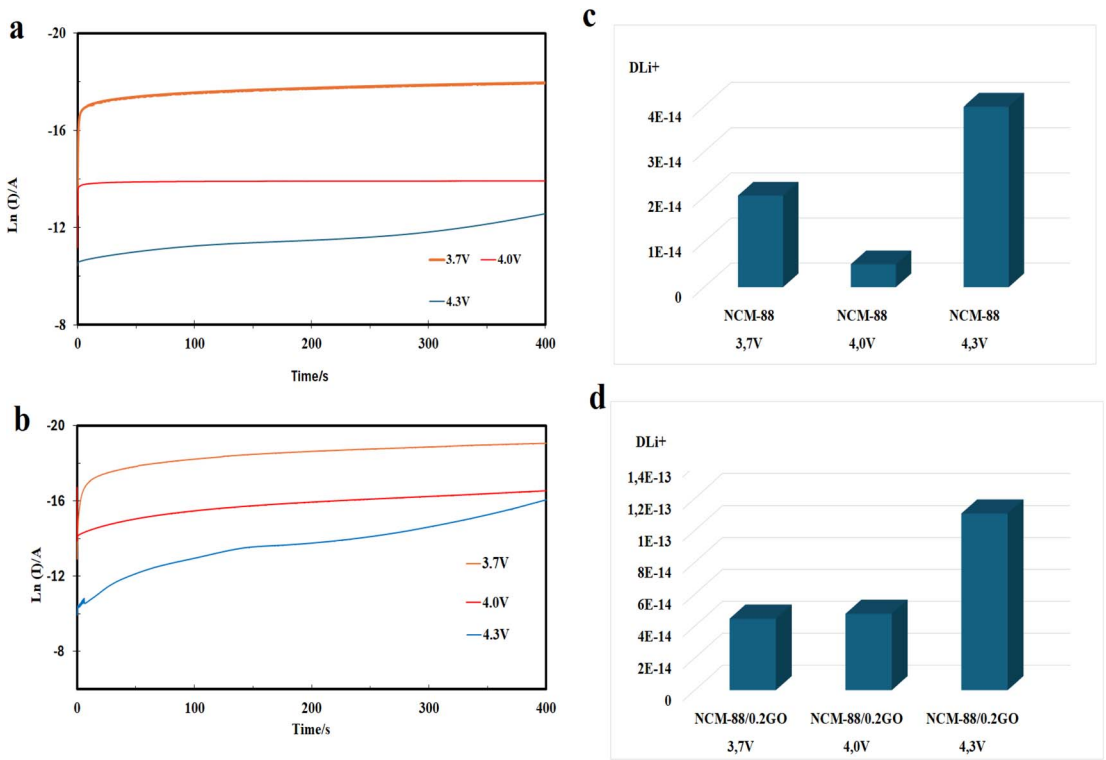

Fig. 8 Transient current plots of PITT: ln(*I*) *vs.* *t* of (a) NCM-88 and (b) NCM-88/0.2GO. D_{Li^+} obtained from the PITT data at different potentials for (c) NCM-88 and (d) NCM-88/0.2GO.

NCM-88/0.2% has an enhanced rate capability compared to pristine NCM-88. Specifically, NCM-88/0.2% retains 98% of its initial capacity at 0.1C, compared to 96.7% for pristine NCM-88, demonstrating superior rate performance and suggesting improved Li^+ migration kinetics due to the optimized coating layer.

To examine how the GO coating layer influences the kinetic behavior of lithium-ion diffusion (D_{Li^+}), the PITT analysis of NCM-88 and NCM-88/0.2GO is compared in Fig. 8. The D_{Li^+} value is determined from the slope of the linear segment in the ln[$I(t)$] *vs.* *t* curve:

$$D_{Li^+} = -\frac{4L^2}{\pi^2}\frac{\mathrm{d}\ \ln[I(t)]}{\mathrm{d}t}$$

L represents the lithium-ion diffusion length, which is approximately equal to the primary particle size of the material. Both samples exhibit similar D_{Li^+} curves, and the D_{Li^+} values increase as the potential rises. However, after GO coating, the chemical diffusion coefficient of lithium ions shows a significant improvement. For NCM-88, the D_{Li^+} value falls within the range of approximately 10^{-15} to 10^{-14} $cm^2\ s^{-1}$, whereas for NCM-88/0.2GO, it is enhanced to 10^{-13} to 10^{-14} $cm^2\ s^{-1}$. This increase in D_{Li^+} is attributed to the fast ionic conductivity of the GO layer.

Electrochemical impedance spectroscopy (EIS) measurements were conducted to further investigate the role of the GO coating layer in the electrode performance. The Nyquist plots obtained after the first cycle and after 62 cycles are presented in Fig. 9, with Fig. 9c illustrating the corresponding equivalent electrical circuit. The high- and medium-frequency semicircles correspond to the resistance of the solid electrolyte interphase (SEI) layer (R_{sf}) and the charge transfer resistance at the electrode/electrolyte interface (R_{ct}), respectively. Meanwhile, the inclined line in the low-frequency region represents the Warburg impedance (Wo), which is associated with the solid-state diffusion of lithium ions within the cathode material. The extracted resistance values are summarized in Table 3. In the equivalent circuit, the solution resistance of the cell is denoted as R_s, whereas CPE1 and CPE2 represent the non-ideal capacitances of the surface layer and the electrical double-layer, respectively. As shown in Table 3, the GO coating effectively reduces R_{sf}, indicating a lower lithium-ion migration resistance across the SEI layer. Additionally, during prolonged cycling, R_{sf} in the pristine NCM-88 electrode exhibits a more rapid increase compared to the GO-coated material. Notably, the R_{sf} growth in NCM-88/0.2GO is significantly lower than in uncoated NCM-88, increasing from 9.7 Ω to 14.9 Ω after 62 cycles, highlighting the stability and enhanced electrochemical performance of the GO-modified electrode. Furthermore, the GO coating also mitigates the increase in R_{ct} during cycling, a phenomenon that is particularly pronounced in the NCM-88/0.2GO electrode. For instance, the R_{ct} of NCM-88/0.2GO exhibits only a moderate increase from 13.7 Ω to 57.4 Ω over cycling, whereas the R_{ct} of pristine NCM-88 rises sharply from 42.9 Ω to 144.2 Ω. This significant increase in R_{ct} for the uncoated electrode can be attributed to direct contact between the NCM material and the electrolyte, which accelerates the dissolution of transition metal ions and promotes the formation of impurity phases during the charge–discharge process. Consequently, these side reactions

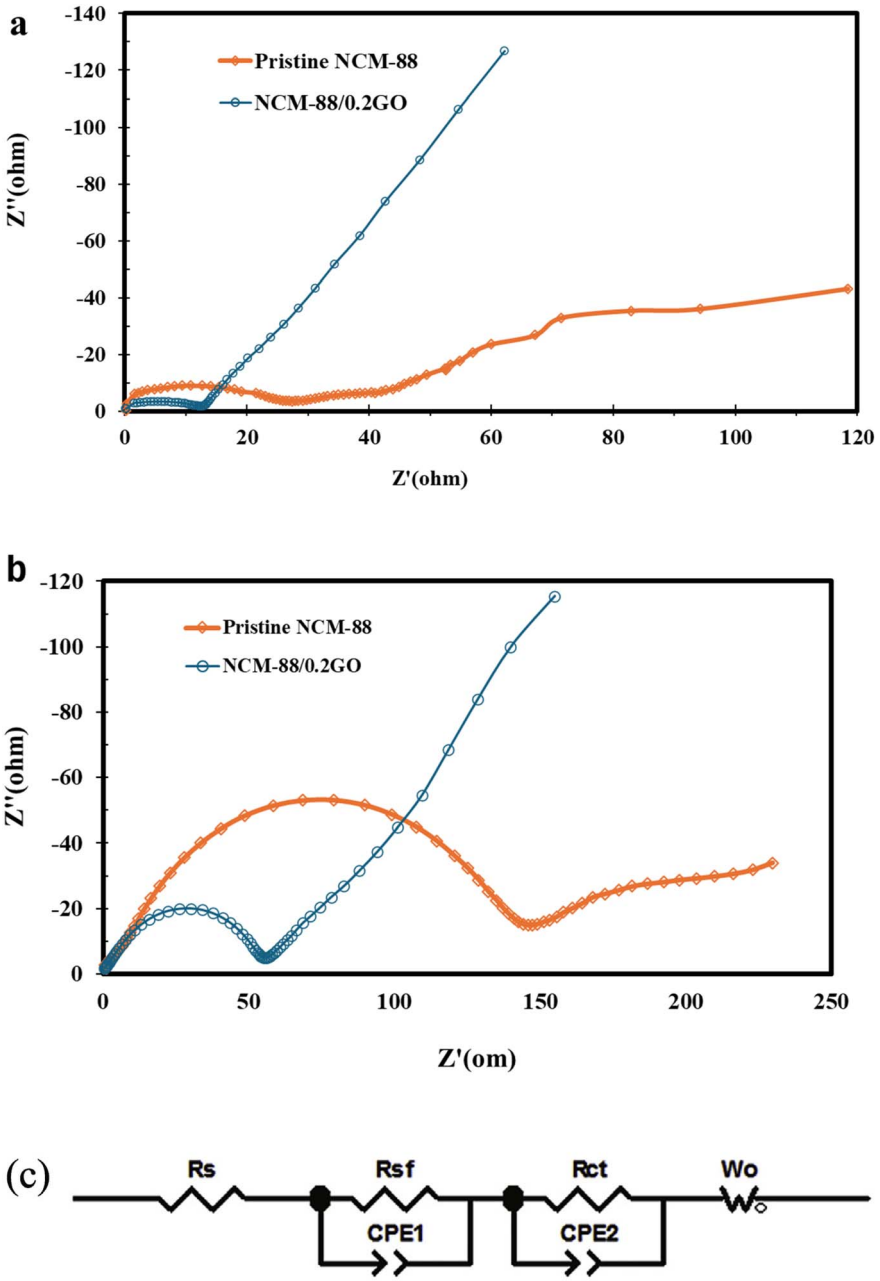

Fig. 9 EIS plots of the NCM-88 and NCM-88/0.2GO (a) before and (b) after 62 cycles; (c) the equivalent electrical circuit.

Table 3 The fitted EIS parameters for NCM-88 and NCM-88/0.2GO samples after 1st and 62nd cycles

	R_{sf}/Ω		R_{ct}/Ω	
Sample	1st	62nd	1st	62nd
NCM-88	26.8	43.8	42.9	144.2
NCM-88/0.2GO	9.7	14.9	13.7	57.4

contribute to a substantial increase in charge transfer resistance.

The results of this analysis clearly demonstrate that the GO coating layer effectively suppresses undesirable interfacial reactions between the electrode and the electrolyte. As a result, it significantly reduces both SEI resistance and charge transfer resistance throughout cycling. This reduction in resistance is a key factor contributing to the enhanced cycling stability and improved electrochemical performance of the GO-coated electrode.

Graphite anode materials were used in Pouch cell electrodes. Fig. 10b illustrates the charge/discharge cycling performance of the coated NCM-88 cathode materials at a current density of 1C, within a voltage range of 2.8 V to 4.3 V, and at 25 °C. The NCM-88/0.2 wt% GO initially displayed a discharge capacity of 189.4 mA h g^{-1}, which decreased to 171.3 mA h g^{-1} after 1000 cycles. The corresponding specific discharge capacity retention

rate was 90.3%, indicating that the GO-coated materials exhibited excellent capacity retention. To better understand the performance of NCM-88 coated with 0.2 wt% GO, Table 4 compares the electrochemical characteristics of this study and other various compositions, including their potential window, rate/discharge capacity, and capacity retention over specific cycles. The comparison highlights the superior cycle stability and capacity retention of the GO-coated NCM-88 in contrast to pristine and modified NCM compositions. For instance, this study demonstrates that the GO-coated NCM-88 achieves a discharge capacity of 171.3 mA h g^{-1} at 1C after 1000 cycles and retains 90.3% of its capacity over 1000 cycles. In contrast, pristine $Ni_{0.88}Co_{0.06}Mn_{0.06}O_2$ within the same potential window retained only 59.8% of its capacity at 1C after 200 cycles. Similarly, $Ni_{0.88}Co_{0.06}Mn_{0.06}O_2$@$TiNb_2O_7$-Ti showed a higher discharge capacity (181.2 mA h g^{-1} at 1C after 200 cycles) but lower capacity retention (87.9%) compared to this study. $Ni_{0.88}Co_{0.06}Mn_{0.06}O_2$@Nb, demonstrated a capacity of 156.5 mA h g^{-1} at 0.5C after 200 cycles with retention of 84.53%. Other compositions, such as graphene, Na/Al, and Al–B coatings, also exhibit varying improvements in performance metrics, though none match the combination of high capacity, and outstanding long-cycle retention after 1000 cycles seen in this study. The above results indicate that the dry coating strategy used in this work effectively enhances overall electrochemical performance. This leads to the assumption that the surface engineering effect may be altered or optimized by controlling the degree of chemical interaction between GO nanoparticles and surface species, a phenomenon often overlooked. Commonly, higher coating amounts (such as the 1 wt% case in this study) are thought to result in less improved performance without considering the different chemical changes that occur with excess coating precursors. GO and its reduced form can improve the formation and stability of the cathode electrolyte interface (CEI) in LIBs, leading to enhanced cycling performance and reduced capacity fade. The functional

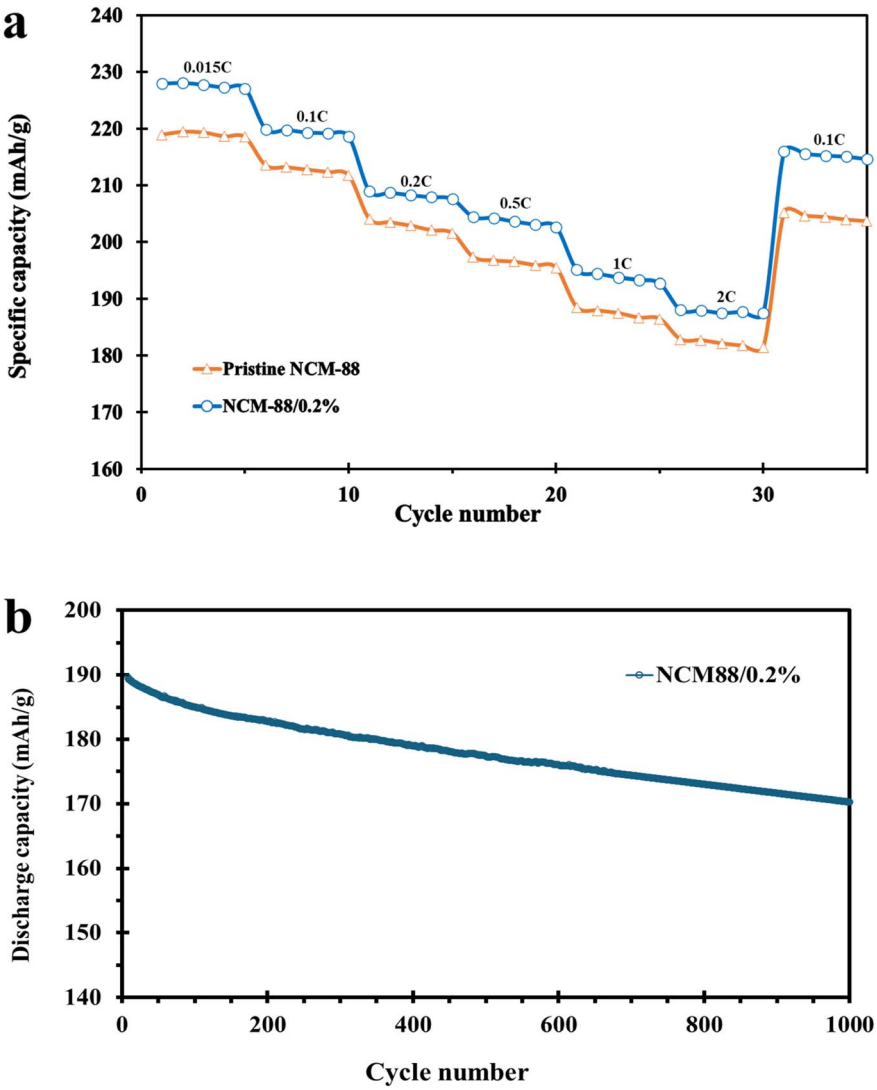

Fig. 10 (a) Rate capability of pristine NCM-88 and NCM-88/0.2% during the discharge and (b) discharge cyclic performance of NCM-88/0.2% at 1C and 25 °C.

Table 4 Electrochemical Performance comparison of GO-coated NCM-88 and other NCM-based cathode materials

Compositions	Window potential (V *vs.* Li/Li^+)	Rate/discharge capacity [mA h g^{-1}]/cycles	Rate/capacity retentions/cycle number	Ref.
$Ni_{0.88}Co_{0.09}Mn_{0.03}O_2$@0.2%GO	2.8–4.3	1C/171.3/after 1000	1C/90.3%/1000	This study
Pristine $Ni_{0.88}Co_{0.06}Mn_{0.06}O_2$	3–4.3	1C/124.3/after 200	1C/59.8%/200	49
$Ni_{0.88}Co_{0.06}Mn_{0.06}O_2$@$TiNb_2O_7$-Ti	3–4.3	1C/181.2/after 200	1C/87.9%/200	49
$Ni_{0.888}Co_{0.056}Mn_{0.056}O_2$@Nb	2.8–4.3	0.5C/156.5/after 200	0.5C/84.53%/200	50
$Ni_{0.88}Co_{0.08}Mn_{0.04}O_2$@Graphene	2.7–4.4	3C/160/after 50	1C/77.8%/100	51
Pristine $Ni_{0.88}Co_{0.08}Mn_{0.04}O_2$	2.8–4.3	1C/170.5/after 50	1C/79%/50	52
$Ni_{0.88}Co_{0.08}Mn_{0.04}O_2$@Na/Al	2.8–4.3	1C/180.4/after 50	1C/84%/50	52
$Ni_{0.88}Co_{0.06}Mn_{0.06}O_2$@Al-B	2.4–4.3	0.5C/148.7/after 250	0.5C/75.5%/250	53
Pristine $Ni_{0.88}Co_{0.09}Mn_{0.03}O_2$	2.8–4.3	1C/156.2/after 300	1C/88.3%/300	20
$Ni_{0.88}Co_{0.09}Mn_{0.03}O_2$@ZSM-5	2.8–4.3	1C/165.4/after 300	1C/90.9%/300	20
Pristine $Ni_{0.88}Co_{0.09}Mn_{0.03}O_2$	2.75–4.4	0.5C/142/after 1000	0.5C/69%/1000	54
$Ni_{0.88}Co_{0.09}Mn_{0.03}O_2$@$Li_{1.4}Y_{0.4}Ti_{1.6}(PO_4)_3$	2.75–4.4	0.5C/170/after 1000	0.5C/85%/1000	54
$Ni_{0.88}Co_{0.09}Mn_{0.03}O_2$@ Al/Zr	2.75–4.4	0.5C/161/after 150	0.5C/83.4%/150	55
$Ni_{0.8}Co_{0.1}Mn_{0.1}O_2$ @MTP	2.7–4.5	1C/179.5/after 200	1C/89.3%/200	56

groups on GO interact with the electrolyte, while heat treatment improves its conductivity. The influence of coating on the formation of the CEI can be investigated based on insights from previous literature, which provide a foundation for understanding its impact on electrochemical performance and interfacial stability.[57,58]

4. Conclusions

In summary, this study demonstrates a facile and effective dry coating method for the surface modification of NCM-88 using GO. Using high-energy mixing, a nanoscale graphene oxide coating layer successfully forms on the Ni-rich cathode surface, optimizing electrochemical performance by facilitating Li^+ migration and protecting the cathode from adverse reactions. The GO coating improves electrochemical performance, including enhanced rate capability, increased initial discharge capacity, and improved capacity retention. Characterization techniques confirm the uniform and amorphous nature of the GO coating, which does not alter the pristine morphology of the NCM-88 particles. Among the various GO coating thicknesses studied, the 0.2 wt% GO-coated NCM-88 shows the optimal balance, achieving the highest performance. This work highlights the potential of GO surface modification to improve the efficiency and longevity of Ni-rich cathode materials in LIBs.

Data availability

The data supporting the findings of this study are available on Zenodo *via* this link: **https://zenodo.org/records/15275067**.

Conflicts of interest

There are no conflicts to declare.

Acknowledgements

This work was supported by BATCircle3.0 (Business Finland 2196/31/2024). This project has received funding from the European Union's Horizon Europe Research and innovation program under Grant Agreement No. 101147342 (SAFELOOP). Dr Palanivel Molaiyan gratefully acknowledges financial support from the Research Council of Finland (Academy Research Fellows 2024, Project In2BaT, grant no. 362298). Jaakko Pulkkinen is acknowledged for his help with the heat treatment of the materials, as well as the staff at the Centre for Material Analysis University of Oulu for the measurement of the samples.

References

1 B. Scrosati and J. Garche, *J. Power Sources*, 2010, **195**, 2419–2430, DOI: **10.1016/j.jpowsour.2009.11.048**.
2 Y. Chen, T. Wang, H. Tian, D. Su, Q. Zhang and G. Wang, *Adv. Mater.*, 2021, **33**, 202003666, DOI: **10.1002/adma.202003666**.
3 Y. Zhang, N. Hao, X. Lin and S. Nie, *Carbohydr. Polym.*, 2020, **234**, 115888, DOI: **10.1016/j.carbpol.2020.115888**.
4 H. Rostami, J. Valio, P. Suominen, P. Tynjälä and U. Lassi, *Chem. Eng. J.*, 2024, **495**, 153471, DOI: **10.1016/j.cej.2024.153471**.
5 J. He, J. Meng and Y. Huang, *J. Power Sources*, 2023, **570**, 232965, DOI: **10.1016/j.jpowsour.2023.232965**.
6 M. Armand, P. Axmann, D. Bresser, M. Copley, K. Edström, C. Ekberg, D. Guyomard, B. Lestriez, P. Novák, M. Petranikova, W. Porcher, S. Trabesinger, M. Wohlfahrt-Mehrens and H. Zhang, *J. Power Sources*, 2020, 228708, DOI: **10.1016/j.jpowsour.2020.228708**.
7 H. Cavers, P. Molaiyan, M. Abdollahifar, U. Lassi and A. Kwade, *Adv. Energy Mater.*, 2022, **12**, 202200147, DOI: **10.1002/aenm.202200147**.
8 P. Molaiyan, S. Bhattacharyya, G. S. dos Reis, R. Sliz, A. Paolella and U. Lassi, *Green Chem.*, 2024, **26**, 7508–7531, DOI: **10.1039/d3gc05027k**.
9 X. Feng, Z. Yang, D. Tang, Q. Kong, L. Gu, Z. Wang and L. Chen, *Phys. Chem. Chem. Phys.*, 2015, **17**, 1257–1264.
10 J. Hwang, K. Do and H. Ahn, *Chem. Eng. J.*, 2021, 126813, DOI: **10.1016/j.cej.2020.126813**.

11 R. Jung, M. Metzger, F. Maglia, C. Stinner and H. A. Gasteiger, *J. Electrochem. Soc.*, 2017, **164**, A1361–A1377.
12 H. H. Sun and A. Manthiram, *Chem. Mater.*, 2017, **29**, 8486–8493.
13 P. Yan, J. Zheng, J. G. Zhang and C. Wang, *Nano Lett.*, 2017, **17**, 3946–3951, DOI: **10.1021/acs.nanolett.7b01546**.
14 A. Mohanan Pillai, P. S. Salini, B. John, S. Sujatha and T. Mercy, *Chem. Rec.*, 2023, **23**, e202300132.
15 J. Yan, H. Huang, J. Tong, W. Li, X. Liu, H. Zhang, H. Huang and W. Zhou, *Interdiscip. Mater.*, 2022, **1**, 330–353.
16 H. H. Sun, H. H. Ryu, U. H. Kim, J. A. Weeks, A. Heller, Y. K. Sun and C. B. Mullins, *ACS Energy Lett.*, 2020, **5**, 1136–1146, DOI: **10.1021/acsenergylett.0c00191**.
17 W. Yan, S. Yang, Y. Huang, Y. Yang and G. Yuan, *J. Alloys Compd.*, 2020, **819**, 153048, DOI: **10.1016/j.jallcom.2019.153048**.
18 P. Guan, L. Zhou, Z. Yu, Y. Sun, Y. Liu, F. Wu, Y. Jiang and D. Chu, *J. Energy Chem.*, 2020, **43**, 220–235, DOI: **10.1016/j.jechem.2019.08.022**.
19 L. Zhao, G. Chen, Y. Weng, T. Yan, L. Shi, Z. An and D. Zhang, *Chem. Eng. J.*, 2020, 126138, DOI: **10.1016/j.cej.2020.126138**.
20 H. Rostami, P. Mehdipour, T. Hu, J. Välikangas, T. Kauppinen, P. Laine, U. Lassi, R. Sliz and P. Tynjälä, *Ind. Eng. Chem. Res.*, 2024, 8847–8859, DOI: **10.1021/acs.iecr.3c04400**.
21 F. Ma, Y. Wu, G. Wei, S. Qiu and J. Qu, *J. Solid State Electrochem.*, 2019, **23**, 2213–2224.
22 R. S. Negi, Y. Yusim, R. Pan, S. Ahmed, K. Volz, R. Takata, F. Schmidt, A. Henss and M. T. Elm, *Adv. Mater. Interfaces*, 2021, 2101428, DOI: **10.1002/admi.202101428**.
23 J. Wang, Y. Yu, B. Li, T. Fu, D. Xie, J. Cai and J. Zhao, *Phys. Chem. Chem. Phys.*, 2015, **17**, 32033–32043.
24 A. M. Pillai, P. S. Salini, G. Rekha Krishnan, A. Chithra, B. John, S. Pillai, S. SarojiniAmma and M. T. Devassy, *J. Alloys Compd.*, 2024, 173064, DOI: **10.1016/j.jallcom.2023.173064**.
25 L. An, W. Li, J. Wang, S. Liu, K. Jiao, L. Fan, J. Liang, Z. Liu and Q. Du, *Appl. Energy*, 2024, 122272, DOI: **10.1016/j.apenergy.2023.122272**.
26 W. Kang, A. Jiang, S. Chen, X. Cao, X. Yu, Y. Luo and W. Deng, *J. Alloys Compd.*, 2024, 172700, DOI: **10.1016/j.jallcom.2023.172700**.
27 B. Li, C. Pan, Y. Zhai, W. Zou, H. Yin, X. He and Y. Gao, *Mater. Lett.*, 2024, 135797, DOI: **10.1016/j.matlet.2023.135797**.
28 S. Y. Lee, J. H. Park, J. H. Cho, S. B. Kim, W. S. Kim and S. Y. Lee, *J. Mater. Chem.*, 2012, **22**, 12574–12581.
29 W. Jiang, Y. Jiang and C. Huang, *ACS Omega*, 2024, 21006–21015, DOI: **10.1021/acsomega.4c00301**.
30 S. She, Y. Zhou, Z. Hong, Y. Huang and Y. Wu, *ACS Omega*, 2022, **7**, 24851–24857.
31 L. Zhou, H. Yang, T. Han, Y. Song, G. Yang and L. Li, *Front. Chem.*, 2022, **10**, 914930, DOI: **10.3389/fchem.2022.914930**.
32 K. Li, B. Lin, Q. Li, H. Wang, S. Zhang and C. Deng, *Anchoring Iodine to N-Doped Hollow Carbon Fold-Hemisphere: Toward Fast and Stable Cathode for Rechargeable Lithium–Iodine Batteries*, 2017.
33 Q. Hou, G. Cao, P. Wang, D. Zhao, X. Cui, S. Li and C. Li, *J. Alloys Compd.*, 2018, **747**, 796–802.
34 S. Xia, Q. Guo, Y. Yu, Y. Li, S. Wang, D. Dong, Z. Liu, H. Zhou, X. Zhou and Z. Liu, *Carbon*, 2023, **203**, 743–752.
35 Z. Wang, S. Zhuang, G. Sun, X. Pan, J. He, Y. Sun, S. Jiang and Y. Ren, *Diamond Relat. Mater.*, 2023, 110233, DOI: **10.1016/j.diamond.2023.110233**.
36 C. Yang, X. Zhang, M. Huang, J. Huang and Z. Fang, *ACS Appl. Mater. Interfaces*, 2017, **9**, 12408–12415.
37 J. Ma, C. Wang and S. Wroblewski, *J. Power Sources*, 2007, **164**, 849–856.
38 K. C. Kil, G. Y. Kim, C. W. Cho, M. D. Lim, K. Kim, K. M. Jeong, J. Lee and U. Paik, *Electrochim. Acta*, 2013, **111**, 946–951.
39 W. Bauer, D. Nötzel, V. Wenzel and H. Nirschl, *J. Power Sources*, 2015, **288**, 359–367.
40 X. Chen, W. Lu, C. Chen and M. Xue, *Int. J. Electrochem. Sci.*, 2018, **13**, 296–304.
41 J. Hwang, K. Do and H. Ahn, *Chem. Eng. J.*, 2021, 126813, DOI: **10.1016/j.cej.2020.126813**.
42 H. Yu, B. Zhang, C. Bulin, R. Li and R. Xing, *Sci. Rep.*, 2016, 36143, DOI: **10.1038/srep36143**.
43 W. Gul and H. Alrobei, *Polymers*, 2021, 1818, DOI: **10.3390/polym13111818**.
44 X. Li, K. Zhang, M. Wang, Y. Liu, M. Qu, W. Zhao and J. Zheng, *Sustainable Energy Fuels*, 2018, **2**, 413–421.
45 F. Wu, J. Tian, Y. Su, J. Wang, C. Zhang, L. Bao, T. He, J. Li and S. Chen, *ACS Appl. Mater. Interfaces*, 2015, **7**, 7702–7708.
46 N. V. Kosova, E. T. Devyatkina and V. V. Kaichev, *J. Power Sources*, 2007, **174**, 965–969.
47 L. Liang, F. Jiang, Y. Cao, G. Hu, K. Du and Z. Peng, *J. Power Sources*, 2016, **328**, 422–432.
48 F. Wu, Q. Shi, L. Chen, J. Dong, J. Zhao, H. Wang, F. Gao, J. Liu, H. Zhang, N. Li, Y. Lu and Y. Su, *Chem. Eng. J.*, 2023, 144045, DOI: **10.1016/j.cej.2023.144045**.
49 X. Qu, H. Huang, T. Wan, L. Hu, Z. Yu, Y. Liu, A. Dou, Y. Zhou, M. Su, X. Peng, H. H. Wu, T. Wu and D. Chu, *Nano Energy*, 2022, 106665, DOI: **10.1016/j.nanoen.2021.106665**.
50 Y. Li, D. Gao, C. Chang and J. Zheng, *J. Energy Storage*, 2023, 109139, DOI: **10.1016/j.est.2023.109139**.
51 Y. Lee, I. H. Son and K. Park, *J. Power Sources*, 2024, 234450, DOI: **10.1016/j.jpowsour.2024.234450**.
52 H. Gyu Park, K. Min and K. Park, *ACS Appl. Mater. Interfaces*, 2022, **14**, 5168–5176.
53 V. C. Ho, M. Hong, T. B. T. Hoang, T. T. Mai and J. Mun, *Mater. Today Energy*, 2023, 101329, DOI: **10.1016/j.mtener.2023.101329**.
54 X. Fan, X. Ou, W. Zhao, Y. Liu, B. Zhang, J. Zhang, L. Zou, L. Seidl, Y. Li, G. Hu, C. Battaglia and Y. Yang, *Nat. Commun.*, 2021, 5320, DOI: **10.1038/s41467-021-25611-6**.
55 X. Ou, T. Liu, W. Zhong, X. Fan, X. Guo, X. Huang, L. Cao, J. Hu, B. Zhang, Y. S. Chu, G. Hu, Z. Lin, M. Dahbi, J. Alami, K. Amine, C. Yang and J. Lu, *Nat. Commun.*, 2022, 2319, DOI: **10.1038/s41467-022-30020-4**.

56 F. Peng, Y. Chu, Y. Li, Q. Pan, G. Yang, L. Zhang, S. Hu, F. Zheng, H. Wang and Q. Li, *J. Energy Chem.*, 2022, **71**, 434–444.
57 J. Dong, F. Wu, J. Zhao, Q. Shi, Y. Lu, N. Li, D. Cao, W. Li, J. Hao, X. Yang, L. Chen and Y. Su, *Energy Storage Mater.*, 2023, 102798, DOI: **10.1016/j.ensm.2023.102798**.
58 F. Wu, J. Dong, L. Chen, L. Bao, N. Li, D. Cao, Y. Lu, R. Xue, N. Liu, L. Wei, Z. Wang, S. Chen and Y. Su, *Energy Storage Mater.*, 2021, **41**, 495–504.